A02-14237

AIAA 2002–1123

Current Collection to Long Conductors with Wide Geometries for Bare Electrodynamic Tether Applications: A Laboratory Update

Brian E. Gilchrist
University of Michigan, Ann Arbor, Michigan 48109
Sven G. Bilén
The Pennsylvania State University, University Park, Pennsylvania 16802
Alec D. Gallimore, Éric Choiniére, and Daniel Herman
University of Michigan, Ann Arbor, Michigan 48109

40th AIAA Aerospace Sciences Meeting and Exhibit
14–17 January 2002
Reno, Nevada

Current Collection to Long Conductors with Wide Geometries for Bare Electrodynamic Tether Applications: A Laboratory Update

Brian E. Gilchrist*
University of Michigan, Ann Arbor, Michigan 48109
Sven G. Bilén†
The Pennsylvania State University, University Park, Pennsylvania 16802
Alec D. Gallimore‡, Éric Choiniére§, and Daniel Herman¶
University of Michigan, Ann Arbor, Michigan 48109

We describe chamber tests of simulated electrodynamic tethers (EDTs) of different geometries operating in a dense, high-speed plasma. The geometries tested and described here were cylindrical and flat-ribbon. Several important conclusions that can be drawn from the tests are as follows: the currents collected by cylinder are close to what would be predicted via orbital-motion-limited (OML) current collection theory. The tape tether had comparable current levels to a theoretical equal area OML cylinder collector. However, I–V behavior clearly is different at nearest distances (tape width $\sim 16\ \lambda_D$) as compared to furthest test distances (tape width $\sim 6\ \lambda_D$). The tape tether did better than a theoretical equal mass solid cylinder. A "knee" in the I–V curves can be seen in the tape data at a potential that is near the estimated energy of the incoming beam of ions, at least for the closest distances where Debye length is smallest. Below this knee the current increases rapidly as voltage is increased. Above the knee the current increases at a rate near that expected from OML current-collection models depending on the relative width. This likely is an example of high-speed plasma flow effect. Perpendicular tape orientation performed slightly better than parallel starting near the ion beam energy.

Nomenclature

A_p	probe surface area, m^2
d	wire diameter, m
F	thrust, N
g	gravitational acceleration, 9.8 m/s^2
I	total current, A
I_d	thruster discharge current, A
I_E	end-effect current, A
I_p	cylindrical probe current, A
I_{sp}	specific impulse, s
k	Boltzmann's constant, 1.38×10^{-23} J/K
K	end effect to cylindrical probe current ratio
l	tape length, m
m_e	electron mass, 9.109×10^{-31} kg
m_i	ion mass, kg
n_e	electron plasma density, m^{-3}
P	power, W
q	charge magnitude, 1.602×10^{-19} C
r	wire radius, m
t	tape thickness, m
T	wire temperature, K
T_e	electron temperature, K
V_a	applied potential, V
V_d	thruster discharge voltage, V
V_l	thruster loss voltage, V
V_p	plasma potential, V
v_{te}	electron thermal velocity, m/s
w	tape width, m
β	ration of measured currents
ε	spectral emissivity
ε_0	free space permittivity, 8.85×10^{-12} F/m
η	discharge electron current fraction
λ_D	Debye length, m
ρ	resistivity, Ω·cm
σ	Stefan–Boltzmann const., 5.67×10^{-8} W/m^2K^4

Introduction

IT has been predicted that operating in the orbital-motion-limited (OML) regime is especially beneficial for electron current collection to thin, bare electrodynamic tethers (EDTs) with width dimensions on the order of a Debye length.[1] This configuration is different than that of Tethered Satellite System missions (TSS–1 and –1R), which used a large (with respect to λ_D) spherical collector for electron collection.[2] The

*Associate Professor, Electrical Engineering and Space Systems, AIAA Senior Member
†Assistant Professor, Communications and Space Sciences Laboratory, AIAA Member
‡Associate Professor, Aerospace Engineering and Applied Physics, AIAA Associate Fellow
§Graduate Student, Radiation Laboratory, EECS Department
¶Graduate Student, Aerospace Engineering

relative merits of bare tethers versus endbody electron collection is the subject of some debate.[3–6] However, it is likely that one or the other or a combination of both will be most appropriate for differing applications.

As part of NASA's Advanced Space Transportation Program, the Propulsive Small Expendable Deployer System (ProSEDS) mission,[7] which is to fly in 2002, will be the first to use the bare-tether concept and will demonstrate high current and measurable thrust; the technology is also being considered for other future missions. However, a small, thin cylinder is not necessarily the best tether design when considering other practical factors such as tether lifetime. For example, to increase tether lifetime, a tether based on ribbon-like geometry (*e.g.*, flat and wide) or more sparse structures involving interconnected conductor strands; hence, these tethers likely would have dimensions exceeding a Debye length. These new geometries pose several questions that must be addressed before they can be employed. For example, how will the current collection performance change as a function of geometry and Debye length when compared to OML models or when in an ionospheric plasma moving at orbital velocities? Does the orientation of the ribbon with respect to the flowing plasma direction have an impact on collection efficiency?

This work describes two sets of vacuum chamber tests that simulated EDTs of different geometries operating in a dense, high-speed plasma. The geometries described here were cylindrical and flat-ribbon tape. The cylinder sample had a radius ranging 1–3 Debye lengths (as plasma parameters were varied) whereas the tape had a width that ranged from 6–16 Debye lengths. For these tests, the 6-m×9-m chamber operated by Michigan's Plasmadynamics and Electric Propulsion Laboratory (PEPL) was used along with a PEPL/USAF-designed Hall thruster for the plasma source. These tests were done, in part, to support design efforts for future missions after ProSEDS.

OML Current Collection

In the OML regime, the current, i, collected by a conductor in non-flowing plasma is given by the equation

$$i = n_e A_p q \frac{\sqrt{2}}{\pi} v_{te} \left(1 + \frac{qV}{kT_e}\right)^{0.5}, \qquad (1)$$

where V is the applied potential V_a with respect to the plasma potential V_p, i.e., $V = V_a - V_p$. The thermal velocity here is given by $v_{te} = \sqrt{kT_e/m_e}$. For high potentials ($V \gg kT_e/q$), Eqn. 1 reduces to

$$i = n_e A_p q \frac{\sqrt{2}}{\pi} \left(\frac{qV}{m_e}\right)^{0.5}. \qquad (2)$$

We see that for large potentials, the current collected is independent of electron temperature and scales as the square root of the potential.

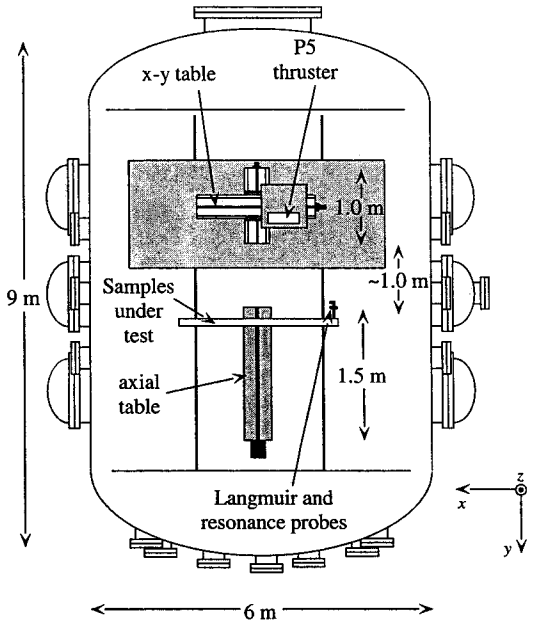

Fig. 1 PEPL LVTF as configured for tests.

Experimental Setup

Chamber Description and Setup

PEPL has as its centerpiece the Large Vacuum Test Facility (LVTF), a cylindrical, stainless-steel-clad tank that is 9 m long and 6 m in diameter.[9] The facility has seven nude cryopumps backed by two 2000 cfm (56,600 l/s) blowers and four 400 cfm (11,300 l/s) mechanical pumps. These pumps give the facility a combined pumping speed of 500,000 l/s on air and 240,000 l/s on xenon and provide the ability to reach a high vacuum ($\sim 10^{-7}$ torr). Fig. 1 is a diagram of the LVTF as it was set up for these tests.

Two positioning tables were used to change the separation distance between the thruster and sample plane and to locate the sample under test (SUT) directly along the thruster's centerline. The thruster was mounted on an x–y table that could move axially 1.0 m and radially sufficient to cover all samples. The samples were mounted on an aluminum frame that was connected to an axial table that could move 1.5 m axially (samples are described in more detail below). Combined table movement allowed thruster-sample separation distance to change from $\sim$ 1 m to $\sim$ 3 m. Changing separation distance was the primary mechanism for changing the plasma density seen at the sample plane.

Samples

Three different sample types were constructed for use during these tests: cylindrical, flat-ribbon tape, and sparse-ribbon or mesh. Only the cylindrical and flat ribbon results are discussed here. Tungsten metal

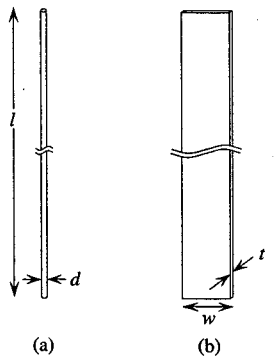

Fig. 2 Schematics of samples used for both test sets: (a) reference cylinder, (b) tape.

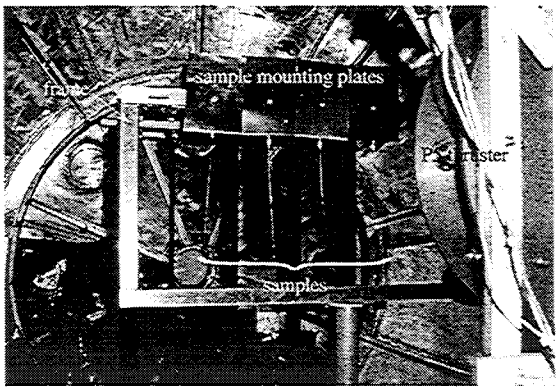

Fig. 3 Picture of the sample support structure for the second test set; structure for the first test set was very similar.

was used for all samples to ensure that they would endure the expected high temperatures, which were caused by the collection of high-energy electrons to the samples' surfaces. During the first set of tests, the samples were approximately 10 cm in length, whereas during the second set of tests, the samples were approximately 30 cm in length. Two tape samples were used in both test sets, one where the width dimension was perpendicular to the plasma flow, the other with the width dimension parallel to the plasma flow. The thickness of the tape was $t = 0.1$ mm. Schematic representation of the samples is given in Fig. 2a-b. Sample descriptions are summarized in Table 1.

All samples were soldered to the center conductor of a bulkhead SHV (safe high voltage) connector; the connector–sample interface was then covered with vacuum epoxy. This sample assembly was then mounted in a piece of stainless-steel flashing, which also functioned as the sample mounting plate. These mounting plates served as localized ground planes and were themselves electrically connected to the sample support frame. For both test sets there existed a minimum of 10-cm clearance between the samples and the frame. A picture of the setup is shown in Fig. 3.

Use of Tungsten for Samples

Due to the energetic electron bombardment of the samples under high potentials, the samples would tend to heat up very quickly, and probably exceed the melting temperature of most metals. Tungsten was therefore used for all samples because it has a melting temperature of 3695 K, which is significantly higher than other metals with low resistivity, such as copper, silver, or gold. Tungsten has a resistivity of $\rho = 5.51 \times 10^{-6}$ Ω·cm, which is within a factor of 2–3 of these other metals.

By performing the following qualitative analysis, we can determine expected worst-case temperatures for the tungsten during current collection. First, we assume the probe is thermally isolated, the surface is equipotential, and finally assume that all electrons collected at the surface (*i.e.*, the electron current to the sample) have been accelerated to the potential of the sample. Then, the power heating the sample is simply $P(V) = I(V)V$, where V is the accelerating potential and the current is a function of V. Fortunately, as the sample's temperature increases, so does its spectral emissivity, ε, which slows down runaway heating slightly. (The electron emission will also increase, but as we show below, for temperatures of our samples, this is negligible.) Using Stefan–Boltzmann's Law, we find the temperature, T, of the wire to be

$$T(V) = \left(\frac{P(V)}{\sigma A \varepsilon}\right)^{0.25}, \qquad (3)$$

From this, we see that T is a function of V. We also note that since P is linearly dependent on A in the OML collection regime and A is found in the denominator of the right-hand side of Eqn. 3, surface area drops out of the equation. What this means is that you are no better or worse off by increasing or decreasing the surface area. Calculations show that at potentials above $\sim$ 300–400 V for the plasma densities of these tests, the tungsten is in danger of melting. Hence, a second temperature mitigation method is needed if potentials higher than these values are used. By pulsing voltages at a low duty cycle, the sample is given a chance to cool off before the next pulse of high voltage heats it. The on-time must be short because the heating occurs quickly, on the order of 10s of milliseconds.

We have considered the possibility of thermionic emission due to wire heating. At the highest applied voltages and positions closest to the thruster, the tungsten samples would briefly glow an orange–yellow color, indicating a temperature $\lesssim$ 2000 K. Maximum possible thermionic emission currents from tungsten can be estimated from the Richardson–Dushman emission equation for a clean metal surface.[10] Even at these

Table 1 Descriptions of Samples Used for Both Test Sets.

	Sample	1	2	3
	Description	Reference Cylinder	Perpendicular Tape	Parallel Tape
first	length, l (cm)	10.0	9.4	9.2
test	Width, w, or	0.28	1.9 (top) to	2.0 (top) to
set	Diameter, d (mm)		2.1 (bottom)	2.2 (bottom)
second	length, l (cm)	29.5	29.5	29.5
test	Width, w, or	0.28	2.0 (top) to	2.0 (top) to
set	Diameter, d (mm)		2.4 (bottom)	2.3 (bottom)

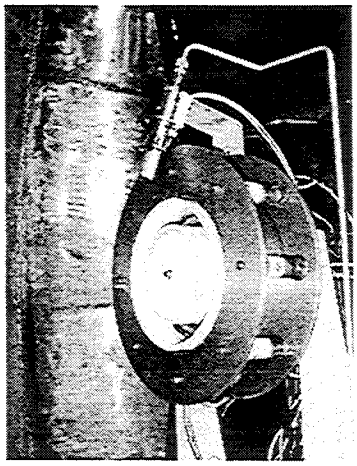

Fig. 4 P5 Thruster.

temperatures, electron emission currents fall below 1 mA/cm^2, which is on the order of 0.5% of the collected current. Indeed, the use of tungsten as emitters has the disadvantage that it must be heated to very high temperatures in order to emit significant levels of current.[10]

Thruster Description and Operating Conditions

The PEPL/AFRL "P5" 5-kW-class Hall-effect thruster was used to provide a flowing plasma for these experiments. A detailed description of the P5 is given by Haas *et al.*[11] and a picture of this thruster is shown in Fig. 4. When operating nominally, the P5 plasma is too fast and dense for the conditions we needed; hence, for these tests the thruster was set at off-nominal conditions in order to lower the plasma velocity and density seen along the thruster's axial direction. The P5 operating conditions for both sets of tests are given in Table 2.

At the time of the tests, the emitted beam energy could only be estimated ($\sim$ 20–50 eV assuming a 100-V discharge voltage) since the discharge voltage was below the nominal thruster operating range and we did not have sensors available to help resolve the character of the P5 flow. Recently, additional tests using laser induced fluorescence (LIF) measurements have allowed us to better estimate bulk and near-field ion beam velocity for the Table 2 conditions.

The LIF measurements used an argon-ion pumped Coherent dye laser system (model 899-29) to characterize the near-field plume plasma of the P5 Hall thruster. This ring dye laser is capable of outputting a continuous, single-frequency beam on the order of 0.1 to 1.0 watt with a line width of 20 MHz from 375 nm (near UV) to 900 nm (near IR). The laser system was used to perform plume diagnostics (velocimetry, relative density, temperature measurements, etc.) on the P5 Hall thruster. The measurements were based on a three-beam multiplex configuration, pioneered by Keefer[13] and expanded by Williams,[14,15] which yields simultaneous azimuthal, axial, and radial velocity components.

The LIF measurements were taken at a distance of 63 cm from the thruster, which, as will be seen, is closer than the zone for the simulated tether measurements. However, because the momentum transfer collision mean-free path was on the order of several meters, these LIF measurements are believed to be representative of our experimental zone near the central axis. The results indicate that for Test-1 power settings the total beam energy along the thruster's boresight was approximately 37 eV and for Test 2 the value was 45 eV. An experimental error of several eV is estimated.

Data Collection and Measurement System

Current–Voltage Measurement System

A schematic of the current–voltage measurement system is given in Fig. 5. The system consisted of a Universal Voltronics BRC 20,000 HV power supply connected to the tether samples by way of a switch box inside the chamber. The HV power supply was controlled via RS–232 by the computer controller running a custom virtual instrument (VI) under LabVIEW. The computer commanded the HV supply to a specified voltage and then quickly back to zero (within 50–100 ms) to minimize sample heating. Before returning to zero, the supply's internal voltage sensor reported back the actual voltage obtained. We verified that the supply pulses were long enough such that the voltage had reached a steady-state value. An

Table 2 Thruster Operating Parameters for Both Test Sets.

Parameter	First Test Set	Second Test Set
Chamber Pressure, Gauge 1 (torr)	1×10^{-5}	6.8×10^{-6}
Chamber Pressure, Gauge 2 (torr)	2×10^{-5}	1.5×10^{-5}
Discharge Voltage, V_d (V)	100	100
Discharge Current, I_d (A)	5.3	4
Inner Magnet Current, I_{im} (A)	2.99	1.04
Outer Magnet Current, I_{om} (A)	1.99	1.03
Cathode Voltage, V_c (V)	−19.7	−19.2
Heater Voltage, V_{htr} (V)	7.1	6.0
Anode Flowrate, $\dot{m}_a$ (sccm)	60	45
Cathode Flowrate, $\dot{m}_c$ (sccm)	6	6

American Aerospace Controls 835–2–10 current sensor (ammeter) was used to measure current. To increase sensitivity, the HV supply line was looped through the sensor 10 times. Since the output of the ammeter was a voltage signal, an HP 34401A voltmeter was used to measure it and, in conjunction with the voltage measurement described above, these values were recorded as voltage–current pairs.

Plasma Parameter Measurements

Three separate probes of two different types were used to measure the plasma environment. Two Langmuir probes (LPs) were mounted as follows: one parallel to the plasma flow and the other perpendicular to the flow. The LP sweeps were made by a Keithley 2410 source electrometer and collected via a custom LabVIEW script using a computer controller (Fig. 5). A resonance probe (RP) was also co-located with the LPs. The resonance probe has been used previously to measure plasma densities in the plume of the P5 thruster.[12] Although still an experimental technique, the RP yields good estimates of density in the far-field region of the P5 plume.

Data

In order to better understand the data presented here, we present first the plasma environment for both test sets and then the data collected during those tests.

Plasma Environment

Fig. 6 reports the measured plasma density and temperature as a function of distance for both test sets. By positioning the sample plane closer and farther from the thruster, we were able to obtain approximately a factor-of-10 change in plasma density. There are several qualifications that must be mentioned concerning the determination of the plasma environment. First, LP data were successfully gathered and analyzed for the first round of tests, but RP data were not collected. The LP data from both the horizontal and vertical probes, which require different analyses due to their orientations, were compared and agreed to within a factor of 2. Unfortunately, during the second test set, the LP data could not be trusted. Hence, we utilized

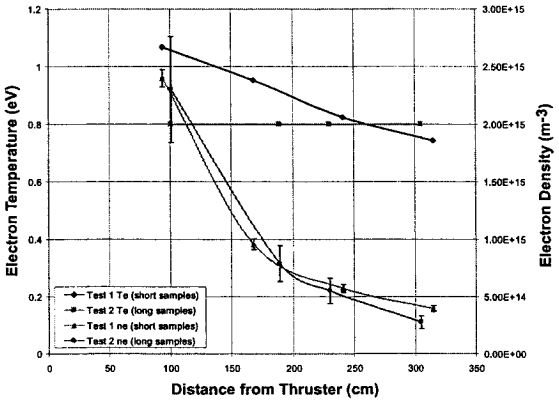

Fig. 6 Plasma parameters measured for both test sets.

RP data exclusively for the 187-, 230-, and 305-cm positions. However, we had to estimate the 100-cm position from the OML current fits. Because the RP does not provide T_e measurements, we were unable to explicitly measure T_e for the second test set, but in comparison with data from the first test set, have set $T_e = 0.8$ eV for all positions. Similarly, the plasma potential could not be estimated from the Langmuir probe data. However, inspection of the cylindrical reference probe data (discussed below) it is estimated that the plasma potential was near 5 V for test 2. Having said this, we feel that we were able to provide an adequate description of the plasma environment for all tests.

Further, at a later time we were able to conduct additional laboratory testing to characterize the conditions summarized in Table 2. In particular, we were able to establish that over at least a ±15-cm radial distance from the central axis there is less than 10% variation in plasma density.

Fig. 7 shows the calculated Debye lengths for both test sets ($\lambda_D = \sqrt{\varepsilon_0 k T_e / q^2 n_e}$). The cylindrical sample had a radius $r = d/2 = 0.14$ mm, so we can see the Debye lengths obtained spanned a range of $\sim$ 1–3 times the cylinder's radius. The tape width of $\sim$ 2–2.4

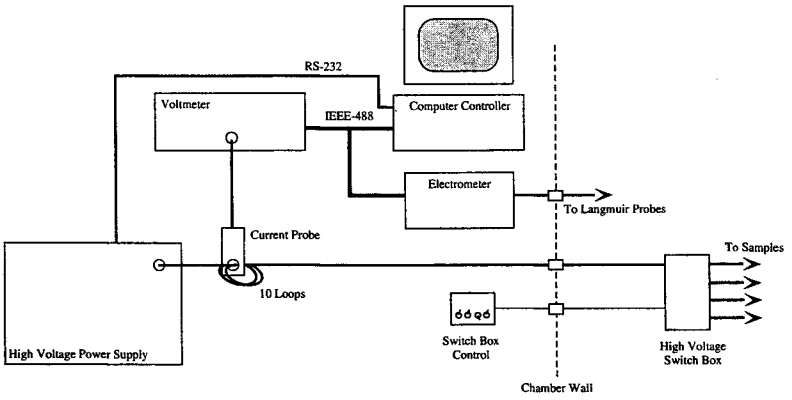

Fig. 5 Schematic of the test equipment setup.

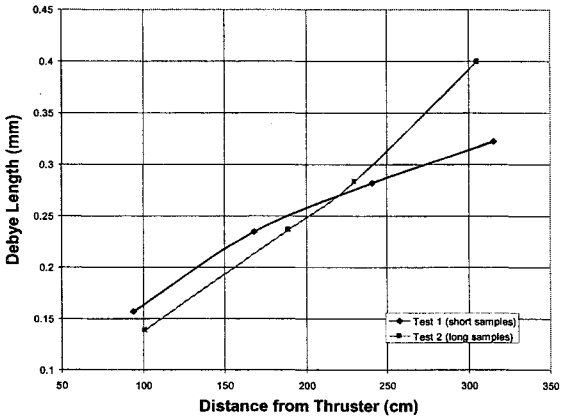

Fig. 7 Debye lengths derived for both test sets.

mm represents from 5–16 times the Debye length. This ability to span from scalelengths on the order of λ_D up to many times λ_D allows us to examine the limits of the OML model of current collection and provides data complementary to that collected by.[25]

We mention at this point several issues regarding the use of the P5 thruster as our plasma source. First, we verified the assumption of a uniform flow along the full length of the test probes using LIF data. This assumption is valid particularly since the probes were placed in the same location with respect to the thruster at a given distance.. Second, any population of slow-moving ions appears not to be a significant factor at least out to 75 cm, the maximum distance of the LIF measurements.

Current Collection Data

This first set of figures (Figs. 8a–d) plots the current as a function of voltage for the tape and cylinder geometries from the second test set at separation distances of 305, 230, 187, and 100 cm, respectively, which represents lower to higher plasma density (see Fig. 6). Note that the zero potential reference point in these plots is the chamber ground, which means tha tthe plasma potential has not been removed. They also include the calculated OML currents to equal area equivalent cylinders (the tape equivalent cylinder radius is approximately 7 mm) assuming a 5-V plasma potential. As the separation distance is reduced, the effective width of the probes in terms of λ_D increases. In general, the calculated model response was near the experimental data. However, the data has important differences in features that will be discussed below. It is also noted that there is some difference between parallel and perpendicular tape orientations.

Fig. 9 provides an example of differences between tests 1 and 2. To compare the differences between the two test runs, given the approximately factor-of-three difference in sample length, the currents obtained in test 1 were multiplied by three before plotting. As seen in the figure, the cylinder samples were approximately the same, however, there is significant difference between the tape tethers. This is possibly due to sample end-effects and is discussed below.

Observations and Analysis

There are several interesting and intriguing observations that result from the data collected during these tests and presented above. From Fig. 8 it can be seen that the perpendicular orientation consistently exceeded the collected current of the parallel orientation and the difference appears to grow at higher densities (shorter Debye lengths). In all cases, the onset of the separation between curves for the different orientations occurred near a threshold of 50-V bias and thus must be independent of plasma density as well as current magnitude. In all but the 100-cm case the difference in current for the orientations appears to reach a constant value that is maintained over the remaining potential range. The 100-cm case appears to show the two curves converging.

We can also describe this separation between the

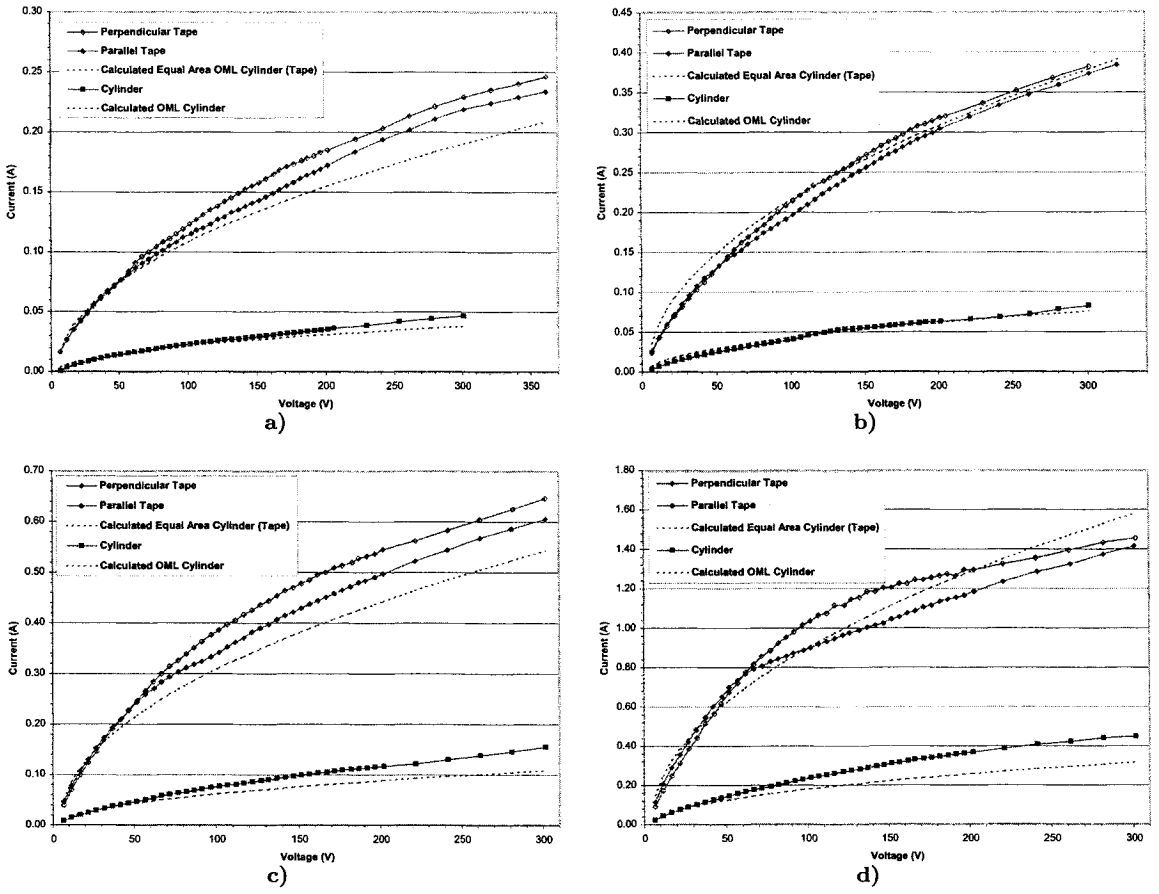

Fig. 8 Current as a function of voltage for the tape and cylinder geometries from the second test set at separation distances of (a) 305 cm, (b) 230 cm, (c) 187 cm, and (d) 100 cm.

parallel and perpendicular tape orientations in terms of a "knee" in the I–V curve for the parallel case that is most pronounced at higher densities (closer distances). A separate knee is suggested at least for the 100-cm perpendicular tape case at a higher potential around 100 V. At potentials below this knee, the current increases rapidly as potential is increased, but not quite as rapid as the OML model. Above the knee for the 305-, 230-, and 187-cm cases, the current increases at a rate that approaches the OML current collection model. For the 100-cm case, the collected current appears to follow a shallower slope than predicted from OML theory.

It is interesting to note that a change in current collection behavior beyond a certain bias threshold was also seen in the TSS–1R[17] and TSS–1 missions[18] where the threshold was at a potential of the ionospheric ion ram kinetic energy. Specifically, the TSS–1R results found that as the satellite potential exceeded the ram kinetic energy of O^+ ions (5.3 eV), the level of kilohertz wave activity increased dramatically[19] and a suprathermal electron population appeared at the satellite's surface.[20] The distributions of wave activity and suprathermal electron fluxes were quite nonuniform around the satellite, indicative of both ram and magnetic field limitations to the current collection. These results were also in qualitative agreement with previously reported results from the TSS–1 mission,[21] but extend over a substantially larger range of currents and satellite potentials. We note that the knee in our case for the parallel orientations, occuring near 50 V in Fig. 8 is very close to the estimate of 45 eV ion beam energy determined via LIF measurements for Test 2, especially when the plasma potential correction is applied. Additional measurements will be required to determine what effects are causing the knee in our response independent of plasma density.

We also note that the predictions for collected current for an equal-area OML cylinder model appears to approximately agree with the collected current for the tape samples even though the width of the tape is much larger than a Debye length (see Fig. 8). Re-

cently reported experimental work by[26] show similar findings. Sanmartín and Estes[22] have considered tape geometries in the OML regime of a stationary, unmagnetized plasma and concluded that there are dimensions beyond a Debye length, depending on potential and plasma temperatures, where a thin tape could satisfy OML collection. Their conclusions for the case appropriate to our experiments would suggest that the tape width could be up to four Debye lengths and still satisfy OML collection. Clearly, we have significantly exceeded this dimension here for our moving plasma. However, a more recent paper by Estes and Sanmartín[23] suggests that their earlier threshold predictions are weak, *i.e.*, degradation in performance is not rapid beyond the theoretical limits. This certainly seems to be the case here. It is possible that the response at 100 cm in Fig. 8 where the tape is $\sim 15\lambda_D$ wide and where the current appears to be following a shallower slope may be indicative of exceeding the OML limit. However, additional experiments will be required to answer this more clearly as it is also possible that we have reached a current level that exceeds what can easily be drawn from the plasma source (1.4 A collected to probe with about 80% of the 4-A discharge current for Test 2 available in the plasma). It is possible that results in Fig. 9 add evidence to this argument as the slope of the Test-1 data (upper pair of curves), which were multiplied by a factor of 3 before plotting, do not have the same fall-off in the rate of increase.

We parenthetically note that the current–voltage responses for the tape samples at 305 and 187 cm in Fig. 8 do seem to be somewhat higher than the equal area OML model response. We have also discussed a possible reason why the 100-cm results could be limited. However, we do not have a clear explanation for the lack of a similar enhancement at 230 cm except possibly experimental error in our estimate of plasma density. More accurate measurements will be needed to address this definitively.

Fig. 9 compares our first and second test runs for the tape and cylinder cases at 94 and 100 cm. Here, the Test 1 current has been multiplied by three to crudely compensate for the fact that the samples were three times shorter than the Test 2 case. We attribute the difference in the tape results as a result of an end-effect even though the Test-1 samples were over $600\lambda_D$ long (end-effects are also multiplied by this same factor of three). In fact, a major reason why the Test-2 run was undertaken was to lengthen the probe samples so as to increase the main probe current relative to the end-effect current.

End effects are well known and they are often modeled by an ideal cylinder for the main portion of the probe with an ideal spherical collector at the end, but the effective radius of the spherical collector is found to be much wider than the actual probe radius[24] and

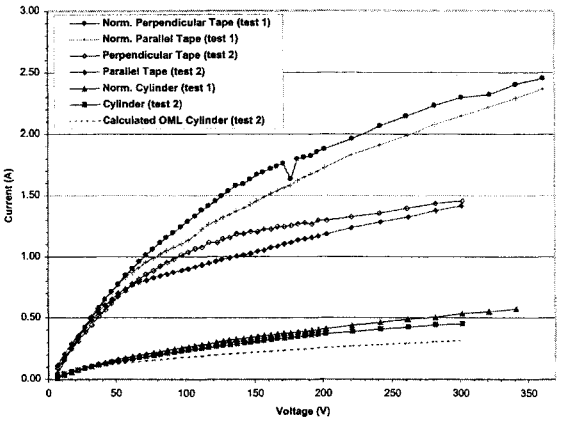

Fig. 9 Comparison of tests 1 and 2.

thus hard to easily model. However, because we have data sets for two different probe lengths, with roughly the same end effects for a given bias potential (this requires the plasma density is the same at the ends of the probe for both data sets), it is possible to quantitatively assess the presence of end effects.

We begin by noting that the voltage dependence of a infinite cylindrical probe would have a $V^{0.5}$ dependence with bias voltage. A spherical collector would have a $V^{1.0}$ relation. We define the ratio of end-effect current to the undisturbed cylindrical probe current as either K_{10} or K_{30} for the 10-cm or 30-cm probes, respectively (test case 1 and 2, respectively) and use as follows:

$$I_{10} = I_{p10} + I_E = I_{p10}(1 + K_{10}), \quad (4)$$

$$I_{30} = I_{p30} + I_E = I_{p30}(1 + K_{30}),$$
$$= 3I_{p10}\left(1 + \frac{K_{10}}{3}\right). \quad (5)$$

where I_{10} and I_{30} are the measured total currents for the two cases at a given bias potential, I_{pxx} is the portion of the total current from an ideal cylindrical probe response, and I_E is the end effect current assumed to be the same for both probes. We define an additional parameter, $\beta = 3I_{10}/I_{30}$, which is the ratio of measured currents with an additional factor of 3 multiplying the 10-cm (test case 1) data. It is then possible to solve for K_{10} in terms of β using Eqns. 4 and 5:

$$K_{10} = \frac{\beta - 1}{1 - \frac{\beta}{3}} \quad (6)$$

If there were no end effect, it would be expected that $\beta = 1$ and $K_{10} = 0$. As a function of bias, we would expect K_{10} to approach zero for low bias potentials and vary with $V^{0.5}$ given the above assumptions for variations of a cylindrical and spherical probe with bias.

Fig. 10 shows a comparison of experimental data and a possible theoretical variation to compare slopes

at the closest distances for Eqn. 6. The expected general character is seen above a minimum voltage, but the power-law variation with bias is somewhat larger than the expected $V^{0.5}$ behavior. The reason for the 0.7 power-law variation as opposed to a 0.5 variation remains to be explained. Nonetheless, these results suggest that end effects are a concern. In future experiments, we plan to use electrical guards at each sample end to minimize end effects, although the mechanical complexity for these small probes is considerable.

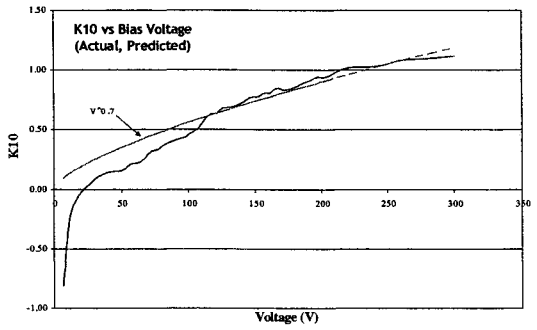

Fig. 10 Variation of predicted end effect currents to ideal cylindrical probe currents (K_{10}) with bias voltage.

Future Tests

We are preparing new experiments to help clarify and expand upon these initial results. First, as stated, we will be including a guard to mitigate against end-effects in all samples. We plan on more fully mapping and characterizing the plume and its energy distribution. We will be increasing the effective width of the tape samples to approximately $30\lambda_D$. We are also planning a series of tests with porous tape samples using holes and slots. The density and geometry of these holes and slots will be varied. It would be useful to determine if turbulent effects are present in the near plasma as the bias is increased beyond the incoming ion beam energy as was seen for TSS–1R. Different beam energies can be used. Magnetic field effects can also be tested.

Conclusions

We believe the experimental results to date in high-speed plasma indicate that the tape tether will be a viable option for bare-tether geometries. Widths well above a Debye length can be used, but we are not able to say yet if there is an experimentally determined maximum dimension as suggested by.[22]

The tape sample current collection appears to generally follow that predicted for an equal-area cylinder OML model. However, the possibility of a small enhancement over the OML equal-area model will have to await additional testing. Further, there is definitely non-OML character present in the data, especially for the 100-cm case. "Knees" in the data appear near the estimated ion beam energy in all cases for the parallel orientation and is therefore independent of plasma density. We note the similarity to TSS–1R data, which also have a change in character of its current–voltage character as the satellite potential exceeded the ram kinetic energy of O^+ ions (5.3 eV). For our simulated tape tether data, any enhancement would seem to be a much smaller factor and will require further testing to identify as will the detection of the presence of any turbulence generated heating of the plasma as the ion beam energy is exceeded. Nonetheless, the knee in the parallel orientation near the ion ram kinetic energy suggests that search for turbulence and plasma heating are warranted. The differences between parallel and perpendicular orientation clearly is an example of high speed flow effect.

The possibility of end-effects even for our longer samples (test 2) does place some question on the overall quantitative assessment of the level of enhancement. In future experiments, a more sophisticated configuration will be used to minimize/eliminate this factor. However, we parenthetically note that adding an end collector may well be a positive enhancement for any bare EDT as our data suggests and suggested by others.[16]

Acknowledgments

The authors would like to thank J. Van Noord and T. Patrick and the PEPL research group for assistance in performing these experiments. The authors thank Drs. D. Cooke, R. Estes, M. Martinez-Sánchez, N. Stone, and K. Wright for useful discussions about these results and their interpretation. This work was performed under contract from The Michigan Technic Corporation and NASA–MSFC.

References

[1]Sanmartín, J. R., Martinez-Sánchez, M., and Ahedo, E. "Bare Wire Anodes for Electrodynamic Tethers," *J. of Prop. and Power*, Vol. 9, No. 3, 1993, pp. 353–360.

[2]Stone, N. H., and Bonifazi, C., "The TSS–1R Mission: Overview and Scientific Context," *Geophysical Research Letters*, Vol. 25, No. 4, 1998, pp. 409–412 (and papers therin).

[3]Johnson, L., Estes, R. D., Lorenzini, E., Martinez-Sanchez, M., Sanmartin, J., "Propulsive Small Expendable Deployer System Experiment," *Journal of Spacecraft and Rockets*, Vol. 37, No. 2, 2000, pp. 173–176.

[4]Van Noord, J., West, B., and Gilchrist, B., "Electrodynamic Tape Tether Performance With Varying Tether Widths at Low Earth Altitudes," AIAA Paper 2001–1141, 39th Aerospace Sciences Meeting and Exhibit, Reno, NV, Jan. 8–11, 2001.

[5]Stone, N. H., and Gierow, P. A., "A Preliminary Assessment of Passive End-body Plasma Contactors [for Electrodynamic Tether Systems]," AIAA Paper 2001–1165, 39th Aerospace Sciences Meeting and Exhibit, Reno, NV, Jan. 8–11, 2001.

[6]Dobrowolny, M., Vannaroni, G., and De Venuto, F., "Electrodynamic Deorbiting of LEO Satellites," *Nuovo Cimento*, Vol. 23C, No. 1, 2000, pp. 85–105.

[7]Johnson, Les, Gilchrist, Brian E., Estes, Robert D., Lorenzini, Enrico, and Ballance, Judy, "Propulsive Small Expendable Deployer System (ProSEDS) Space Experiment," AIAA Paper AIAA–98–4035, 1998.

[8]Forward, R. L., "Failsafe Multistrand Tether Structures for Space Propulsion," AIAA Paper AIAA–92–3214, 1992.

[9]Gallimore, A. D., Kim, S.-W., Foster, J. E., King, L. B., and Gulczinski III, F. S., "Near and Far Field Plume Studies of a One-kilowatt Arcjet," *AIAA J. Prop. Power*, Vol. 12, 1996, pp. 105–111.

[10]Jenkins, R. O., and Trodden, W. G., *Electron and ion emission from solids*, Dover Publications, Inc., New York, 1965.

[11]Haas, James M., Gulczinski III, Frank S., Gallimore, Alec D., Spanjers, Gregory G., and Spores, Ronald A., "Performance Characteristics of a 5 kW Laboratory Hall Thruster," *AIAA Paper AIAA–98–3503*, 1998.

[12]Bilén, Sven G., Haas, James M., Gulczinski III, Frank S., Gallimore, Alec D., and Letoutchaia, Julia N., "Resonance-probe Measurements of Plasma Densities in Electric-propulsion Plumes," AIAA Paper AIAA–99–2714, 1999.

[13]Keefer, D., *et al.*, "Multiplexed Laser Induced Fluorescence and Non-Equilibrium Processes in Arcjets," AIAA paper AIAA–94–2656, 25th Plasmadynamics and Lasers Conference, July 1992.

[14]Williams, G. J., Jr., Smith, T. B., Gulczinski, F. S., Beal, B. E., Gallimore, A. D., and Drake, R. P., "Laser Induced Fluorescence Measurement of Ion Velocities in the Plume of a Hall Effect Thruster," AIAA paper AIAA–1999–2424, 35th Joint Propulsion Conference, 1999.

[15]Williams, G. J., Jr. "The Use of Laser-Induced Fluorescence to Characterize Discharge Cathode Erosion in a 30 cm Ring-Cusp Ion Thruster," Ph.D. Thesis, Dept. of Aerospace Eng., The University of Michigan, September 2000.

[16]Dobrowolny, M., and F. Vannaroni, private communication, 1999.

[17]Thompson, D. C., Bonifazi, C., Gilchrist, B. E., Williams, S. D., Raitt, W. J., Lebreton, J.-P., Burke, W. J., Stone, N. H., and Wright, Jr., K. H., "The Current–Voltage Characteristics of a Large Probe in Low Earth Orbit: TSS–1R Results," *Geophysical Research Letters*, Vol. 25, No. 4, 1998, pp. 413–416.

[18]Katz, I., Melchioni, E., Mandell, M., Oberhardt, M., Thompson, D., Neubert, T., Gilchrist, B., and Bonifazi, C., "Observations of Ionosphere Heating in the TSS–1 Subsatellite Presheath," *J. Geophysical Research*, Vol. 99, No. A5, 1993, pp. 8961–8969.

[19]Iess, L., Harvey, C., Vannaroni, G., Lebreton, J. P., Dobrowolny, M., Manning, R., Cerulli-Irelli, P., Onelli, A., and De Venuto, F. "Plasma Waves in the Sheath of the TSS–1R Satellite," *Geophysical Research Letters*, Vol. 25, No. 4, 1998, pp. 421–424.

[20]Winningham, J. D., Stone, N. H., Gurgiolo, C. A., Wright, K. H., Frahm, R. A., and Bonifazi, C. A., "Suprathermal Electrons Observed on the TSS–1R Satellite," *Geophysical Research Letters*, Vol. 25, No. 4, 1998, pp. 429–432.

[21]Dobrowolny, M., Guidoni, U., Melchioni, E., Vannaroni, C., and Lebreton, J.P., "Current–Voltage Characteristics of the TSS–1 Satellite," *Journal of Geophysical Research*, Vol. 100, No. A12, 1995, pp. 23953–7.

[22]Sanmartín, J. R., and Estes, R. D., "The Orbital-Motion-Limited Regime of Cylindrical Langmuir Probes," *Physics of Plasmas*, Vol. 6, No. 1, 1999, pp. 395–405.

[23]Estes, R. D., and Sanmartín, J. R., "Cylindrical Langmuir Probes Beyond the Orbital-Motion-Limited Regime," *Physics of Plasmas*, Vol. 7, No. 10, 2000, pp. 4320–4325.

[24]Johannig, D., Seifert, W. and Best, A. "Analytic Density Correction for Cylindrical Langmuir Probes Showing End Effects, *Plasma Physics and Controlled Fusion*, Vol. 27, No. 2, 1985, pp. 159–179.

[25]Vannaroni, G., and De Venuto, F., "Current Collection by Bare Tether Samples in a Simulated Ionospheric Environment," Istituto di Fisica dello Spazio Interplanetario CNR, *IFSI–2001–17*, July 2001.

[26]Kruijff, M., van der Heide, E. J., De Venuto, F., Dobrowolny, M., Vannaroni, G., "Long Term Stability of Bare Conductive Tethers: Combined Results from Plasma Chamber Tests and Advanced Simulations," 2001 Space Technologies and Applications International Forum, 2001.